Journal of Crystal Growth 318 (2011) 18–22

Contents lists available at ScienceDirect

Journal of Crystal Growth

journal homepage: www.elsevier.com/locate/jcrysgro

Morphological instability of heteroepitaxial growth on vicinal substrates: A phase-field crystal study

Yan-Mei Yu [a,*], Rainer Backofen [b], Axel Voigt [b]

[a] Institute of Physics, Chinese Academy of Science, P. O. Box 603, 100190 Beijing, China
[b] Institut für Wissenschaftliches Rechnen, Technische Universität Dresden, 01062 Dresden, Germany

ARTICLE INFO

Available online 17 September 2010

Keywords:
A1. Computer simulation
A1. Growth models
A1. Morphological stability
A1. Stress
A1. Substrates
A3. Liquid-phase epitaxy

ABSTRACT

We investigate morphological instability of heteroepitaxially grown thin films on vicinal substrates with the phase-field-crystal (PFC) model. The PFC model is tuned to have a sharp transition between solid and liquid. Thus, steps, terraces and kinks can be clearly identified. The substrate is modeled by an external pining potential. Varying vicinal angle and misfit between substrate and film a phase-diagram for morphological instability of the strained thin film near equilibrium is constructed. The morphology of the growing strained thin film follows the equilibrium morphological phase-diagram, but indicates less critical mismatch strain for dislocation formation. For small mismatch strains, the step-flow and the step-bunching modes contribute to the coherent film growth on the vicinal substrate, whereas for large mismatch strains, the strong non-coherent film growth tendency is caused due to the increased possibility of the mismatch dislocation formation, as companied by the island growth on the hill-and-valley facetted structures. Our simulation results demonstrate interconnection of the steps, the islands, and the mismatch dislocations during the heteroepitaxial growth on the vicinal substrate.

© 2010 Elsevier B.V. All rights reserved.

1. Introduction

In heteroepitaxial growth one material is deposited onto a crystalline substrate formed from a second material. The atomic lattice constant of the deposited material can be different from the substrate, resulting in mismatch strain. Morphological instabilities are induced by the strain, leading to rough surfaces and defects in the film, as known as the Asaro–Tiller–Grinfeld (ATG) instability [1,2]. This phenomenon has been studied intensively using fully continuum models [3–6] and hybrid discrete-continuous step-flow or island dynamics models [7–9]. These methods are computationally saving for modeling large-scale morphologies but with atomic-scale information smeared out. Using the fully atomistic way, the morphological instability of the heteroepitaxially grown thin film has also been investigated based on a solid-on-solid model, i.e., the on-lattice KMC method [10–13]. These KMC simulations are implemented on predefined atomic lattices that rule out any possible atomic defects like voids, overhangs and dislocations. The off-lattice KMC modeling allows atoms freely to locate any continuous spatial positions and has been applied for the study of the morphological instability with atomic defects considered in (1+1) dimensional situations [14,15]. The current effort is focusing on speeding up the off-lattice KMC modeling in order to deal with more complex situations [16]. As another type of atomistic method, molecular dynamics (MD) simulations are also used for modeling film growth morphologies. The time step of the MD simulation is usually small and then growth processes occurring long time cannot easily accessed in MD simulations .

Here we consider a new method known as the phase-field crystal (PFC) model [17–24]. The PFC model has been constructed to describe crystal growth at the atomic length scale but the diffusive time scale. Thus, we are able to simulate long time needed to reach relevant physical processes in heteroepitaxy with the atomic-scale information considered. Elastic and plastic deformations are also considered naturally in the PFC model. The combination of such advantages has demonstrated its great potential in modeling of the heteroepitaxial growth [17,18,20]. In the PFC modeling for heteroepitaxy, a solid is growing on a predefined crystalline substrate with the solid surface in contact with a liquid. This corresponds to the liquid-phase epitaxial film growth, driven by perturbation of the atom number density in the liquid that deviates from equilibrium. Therefore, the property of the PFC solid–liquid interface affects the film growth morphology. In the previous PFC simulations, the solid–liquid interface is usually diffusive, where no atomistic feature is present. However, atomistic features are widely observed in various crystal surfaces. A typical example is vicinal crystal of the surface steps. The stepped configuration changes morphological properties of films grown on the vicinal substrate if compared with that grown on a singular (step-free) or diffusive surface. In this paper, we will

* Corresponding author. Tel.: +86 10 82648059; fax: +86 10 62553698.
E-mail addresses: ymyu@aphy.iphy.ac.cn (Y.-M. Yu), rainer.backofen@tu-dresden.de (R. Backofen), axel.voigt@tu-dresden.de (A. Voigt).

0022-0248/$ - see front matter © 2010 Elsevier B.V. All rights reserved.
doi:10.1016/j.jcrysgro.2010.08.047

explore application of PFC modeling in the sharp solid–liquid interface limit. The steps and other related atomistic growth features are well reflected on the sharp PFC surface. Further, we investigate the heteroepitaxial growth on the vicinal substrate using the PFC modeling. Our simulation results show the interconnected relationship of the steps, the islands, and the mismatch dislocation during the heteroepitaxial growth on the vicinal substrate.

2. Model

In the simplest form [17,18], the PFC model results from the free energy

$$F=\int d\vec{x}\left\{\frac{\psi}{2}[-r+(q^2+\nabla^2)^2]\psi+\frac{\psi^4}{4}+V\psi\right\}, \tag{1}$$

where ψ is a conserved order-parameter field related to the atom number density, r and q are phenomenological parameters, and V is an external potential that is used to define a substrate. It is already known that F is minimized by the constant, hexagonal, and striped phases in two dimensions (2D) and also the bcc, fcc, and hcp phases in three dimensions (3D), depending on the average value $\overline{\psi}$ of ψ and the parameter r. Phase-diagram of the hexagonal phase and the constant phase is shown in Fig. 1. The constant phase corresponds to a supersaturated liquid whose number density deviates from the equilibrium value. Due to the supersaturation, a solid phase (i.e., a film) is precipitated to grow on a prepared substrate. The growth dynamics is governed by

$$\frac{\partial\psi}{\partial t}=\nabla^2(\delta F/\delta\psi)$$
$$=\nabla^2\{[-r+(q^2+\nabla^2)^2]\psi+\psi^3+V\}. \tag{2}$$

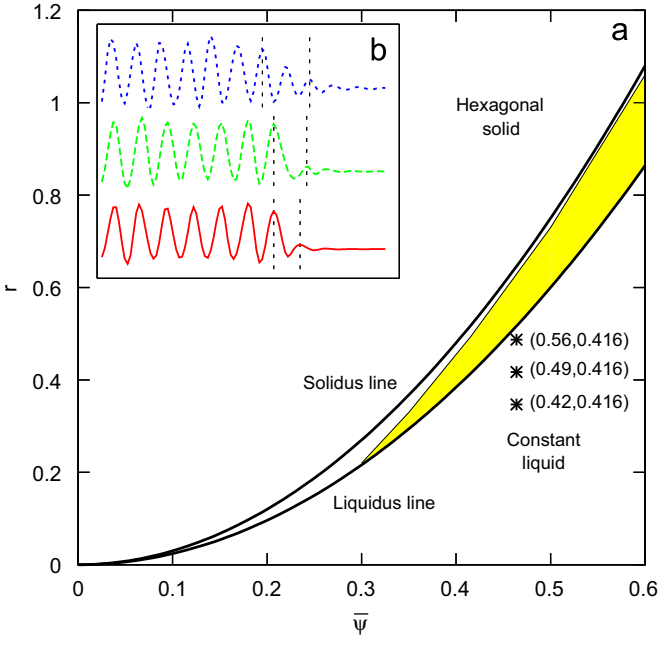

Fig. 1. (a) In the 2D PFC simulation, sharp crystal surface can be obtained using parameters $(r,\overline{\psi})$ in a range denoted by yellow (or gray). (b) Profile of atomic density field spanning the solid and liquid phases. The solid–liquid interface (denoted by parallel dotted lines) is diffusive for $(r,\overline{\psi})=(0.56,0.416)$ (blue-dotted line), but sharp for $(r,\overline{\psi})=(0.49,0.416)$ (green-dash line) and (0.42,0.416) (red-solid line). (For interpretation of the references to color in this figure legend, the reader is referred to the web version of this article.)

Eq. (2) is related to a specific reference state in the liquid state, [23] through

$$q=k_m, \tag{3}$$

$$r=-\frac{k_BT}{\rho_0}\left[\frac{1}{S(k_m)}-\frac{a^2}{4b}\right], \tag{4}$$

$$\psi=\left(\frac{\rho(\vec{x})}{\rho_0}-1-\frac{a}{2b}\right)\sqrt{\frac{b}{3\Gamma}}, \tag{5}$$

with

$$a=\frac{3}{2S(k_m)u_s},\quad b=\frac{4}{30S(k_m)u_s^2},\quad \Gamma=-\frac{k_m^2C''(k_m)}{8}, \tag{6}$$

where $\rho(x)$ is number density field, ρ_0 is atom number density of the reference state, and k_m, $S(k_m)$, and $C''(k_m)$ are peak properties of the liquid structure factor of the reference state, u_s is the amplitude of density waves in the solid. While Eqs. (3)–(6) have suggested a connection of the PFC model to the real system, conducting a PFC simulation for a given material is still a complicated problem that has not been solved completely so far [19]. Here, we shall not focus on a specific material but describe a general approach of PFC modeling for the epitaxial growth on vicinal substrate. A parameter study was performed using Eq. (2). We starts with a solid nucleus in a liquid pool. We choose $(r,\overline{\psi})=(0.56,0.416)$ in the solid region and $(r,\overline{\psi})=(0.49,0.416)$ and (0.42, 0.416) in the solid–liquid coexistence region. These parameters drive solidification of the liquid. The solid–liquid interface appears during solidification. The corresponding atomic density field profiles are shown in Fig. 1(b). The atomic density field profile for (0.56, 0.416) corresponds to an interface that is observed before all liquid has transitioned into the solid phase. The results show that the thickness of the ψ transition zone spanning between the solid and liquid phases changes with $(r,\overline{\psi})$, as illustrated in Fig. 1(b). This thickness can be very small, near one atomic length. The required input values of $(r,\overline{\psi})$ are commonly located at the lower side of the solid–liquid coexistence region in the phase-diagram. For example, the required $(r,\overline{\psi})$ values in 2D PFC simulations are within a range denoted by yellow (or) gray in Fig. 1, for which we can obtain a sharp PFC surface of the step-and-terrace structure.

The numerical dicretization of Eq. (2) is implemented using the semi-implicit Fourier spectral method with a spatial step Δx and a time step Δt. The simulation has been started by placing at the center of the simulation cell a slab of crystalline substrate for heteroepitaxy represented by the external potential V added to the free energy. In the other part of the simulation cell $\psi=\overline{\psi}$ is initialized. The external potential V is added only in the substrate part and disappears outside the substrate. A smooth function is used to smoothen the variation of V in the interface region between the substrate and its neighbored parts. The substrate is prepared by initializing $\psi=\psi_s$, where $\psi_s=A_s[\cos(q_sx)\cos(q_sy/\sqrt{3}))-\cos(2q_sy/\sqrt{3})/2]+\overline{\psi}$ with $A_s=-\frac{4}{5}[\overline{\psi}+\sqrt{15r-36\overline{\psi}^2}/3]$ and $q_s=(\sqrt{3}/2)q_0$ (corresponding to the hexagonal phase) in 2D simulations, or $\psi_s=4A_s(\cos q_sx\cos q_sy+\cos q_sy\cos q_sz+\cos q_sz\cos q_sx)$ with $A_s=-\frac{2}{15}+\frac{1}{15}\sqrt{5\varepsilon-11\overline{\psi}^2}$ and $q_s=(\sqrt{2}/2)q_0$ (corresponding to the bcc phase) in 3D simulations, $q_0=1$, and the coordinates x and y have been rotationally transposed for a vicinal angle θ. Correspondingly, $V=V_0(\psi_s-\overline{\psi})+\overline{\psi}$ is used to pin the atomic lattice of the substrate. The elastic properties of the substrate changes with the magnitude of V_0. For small value such as $V_0=0.5$ the substrate can deform elastically. The rigidity of the substrate converges as the value of V_0 increases. With $V_0=8$ the substrate is rigid perfectly due to the pining potential. Our aim is

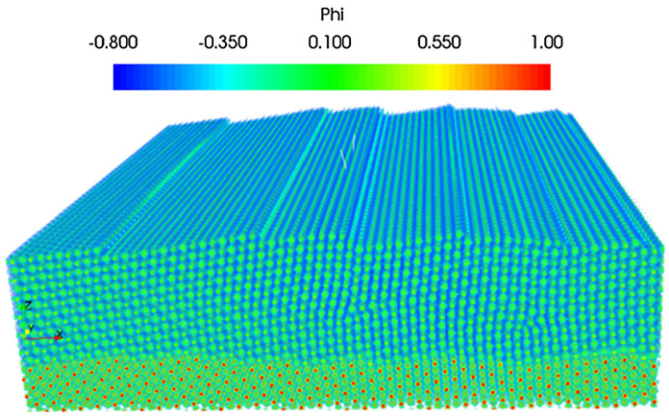

Fig. 2. The heteroepitaxial growth on a vicinal bcc substrate. Red dots on a light-green background corresponds to the substrate, above which is the film. A movie (HeteroepitaxialGrowth.gif) is available online. (For interpretation of the references to color in this figure legend, the reader is referred to the web version of this article.)

the directional growth of the solid on the substrate, hence no random field is used in the liquid. However, in order to check the step stability, we add an initial perturbation of the step spacing on the vicinal substrate. We adopt $q=q_f$ and $q_f<1$, which indicates the mismatch strain between the film and the substrate $\varepsilon=(1-q_f)/q_0$.

Shown in Fig. 2 is a 3D PFC image of the heteroepitaxial growth on a bcc vicinal substrate of a normal miscut by 3.52° away from the (1 1 0) face and towards the [0 0 1] direction, which corresponds to an average monatomic step separation l_s of approximately eight near-neighbor atomic distances ($\sqrt{2}a$, a is atomic lattice constant), simulated using parameters $(r,\overline{\psi},\Delta x,\Delta t)=(0.40,0.426,1.03,0.2)$. This simulated results captures the atomic details of the heteroepitaxial growth on the vicinal substrate, the large-scale step-bunching profile as well as the mismatch dislocations within the film successfully. The simulation corresponding to Fig. 2 (the simulation cell size $L_x\times L_y\times L_z=400\times 400\times 400$) costs a large computer power (72×10 CPU hours at SGI Altix 4700 at TU Dresden. The SGI Altix is based on the dual core Intel Itanium 2 processor, 1.6 GHz). In order to proof the applicability of PFC, we show different growth modes in heteroepitaxy in connection with defect nucleation and defect propagation in detail using 2D PFC simulation. We use $(r,\overline{\psi},\Delta x,\Delta t)=(0.42,0.416,\pi/4,0.2)$, $q_f=$ 0.927–0.99 (corresponding to $\varepsilon=0.073-0.01$), and $\theta=1.66-12.22^\circ$ in the 2D simulations.

3. Results and discussion

We first investigate the morphology near a stationary equilibrium of the heteroepitaxially grown film on the vicinal substrate. Long-time simulation is conducted on a simulation cell of $L_y=400$ boundaried by periodical conditions. The film growth will finally stop due to consumption of mass in the ψ field. A great deal of numerical experiments are conducted for the large range of ε and θ. Diverse growth regimes are obtained, which leads to the regular step-train structure, the step-bunching structure and the faceted hill-and-valley structure with or without dislocations. The results suggest a morphological phase-diagram of the heteroepitaxial growth on the vicinal substrate as functions of ε and θ, as shown in Fig. 3. The boundaries between these different growth morphologies correspond to less ε as θ increases, which indicates the increased stress-induced instability. Fig. 3 can be understood by considering the structure of a vicinal surface. The free energy of a vicinal surface increases with its misorientation θ

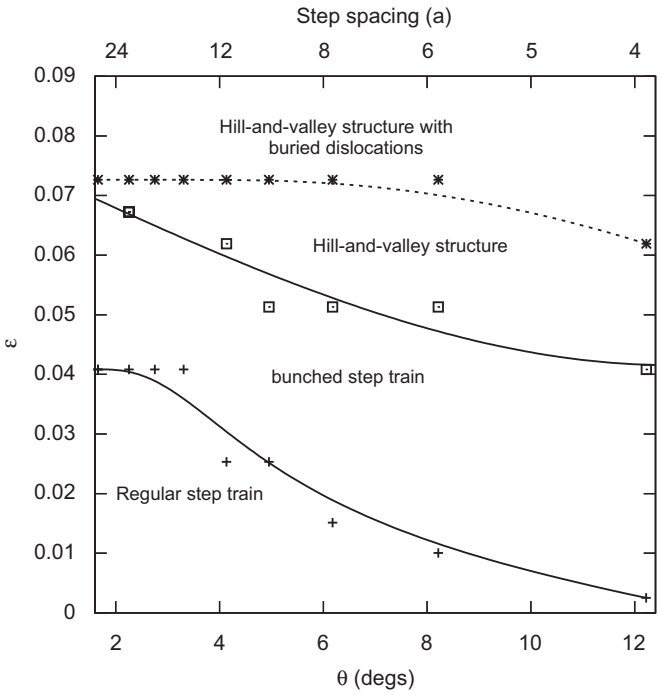

Fig. 3. Morphological phase-diagram of heteroepitaxial growth on the vicinal substrate as functions of mismatch strain ε and vicinal angle θ. The samples +, □, ⁎ denote the critical values of (ε,θ), above which the bunched step train, the hill-and-valley structure, and the hill-and-valley structure with buried dislocations are caused by the stress-induced morphological instability, respectively. The solid and dash lines denote the phase boundaries, which are best fit of these data with +, □, and ⁎.

[25]. In order to decrease the free energy, such a surface has a strong thermodynamics tendency to rearrange the steps into the step-free low-index face, i.e., the step bunching and the step faceting [26]. The vicinal surface of larger θ means the larger step density, where the step growth and its instability prevails. Therefore, the morphological instability of the heteroepitaxial growth on a vicinal substrate changes with the vicinal orientation as a consequence of the unstable step growth induced by the mismatch strain.

We simulate the film growth on a simulation cell of $L_y=1000$ next. The field of ψ is fixed to be $\overline{\psi}=0.416$ at a distance of $L=200$ above the average height of the film, which incorporates a constant mass flux. In this case, the film growth is an approximated constant velocity. The simulated images of the heteroepitaxial growth on the vicinal substrate reproduces the hill-and-valley facet structure, the step bunching, and the regular step-flow on the vicinal substrate, as shown in Fig. 4(a)–(c). The heteroepitaxial growth on a singular substrate is simulated with $\theta=0^\circ$, which is of smooth and stable morphology until for $\varepsilon=0.07$ the rough morphology is shown in Fig. 4(d), indicating the Stranski–Krastanov growth mode. The mismatch dislocations are caused for large ε, see Fig. 4(a) and (d). The mismatch dislocations first originate on the film surface, then glide down to the interface between the film and the substrate. The nucleation pathway of the mismatch dislocation shown in our simulation agrees with the atomic simulation of heteroepitaxy using the off-lattice KMC approach [14]. The dislocation formation releases the elastic stress and then the surface profile is not as rough as for the dislocation-free island growth mode [15].

The surface roughness W and the lateral height–height correlation length L of the heteroepitaxial growth on the vicinal substrate are further illustrated in Fig. 5. The increase of W and L with the film thickness indicates the unstable growth of the

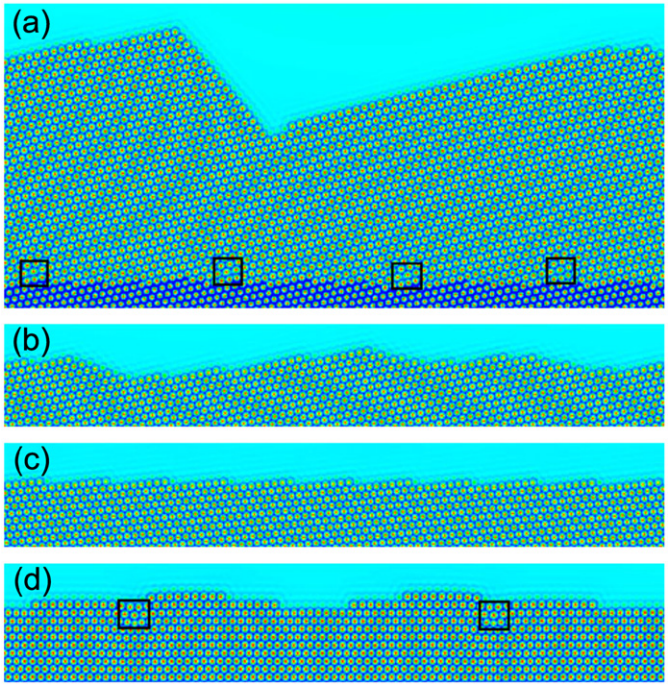

Fig. 4. Morphologies of heteroepitaxial growth simulated for different mismatch strains ε and substrate vicinal angles θ, (a) $\varepsilon=0.06$ and $\theta=12.22^{\circ}$, (b) $\varepsilon=0.025$ and $\theta=12.22^{\circ}$, (c) $\varepsilon=0.025$ and $\theta=6.18^{\circ}$, (d) $\varepsilon=0.07$ and $\theta=0^{\circ}$. Dislocations are enclosed by black squares. Red dots on a dark-blue background is the substrate, see the bottom of (a), above which is the film. (For interpretation of the references to color in this figure legend, the reader is referred to the web version of this article.)

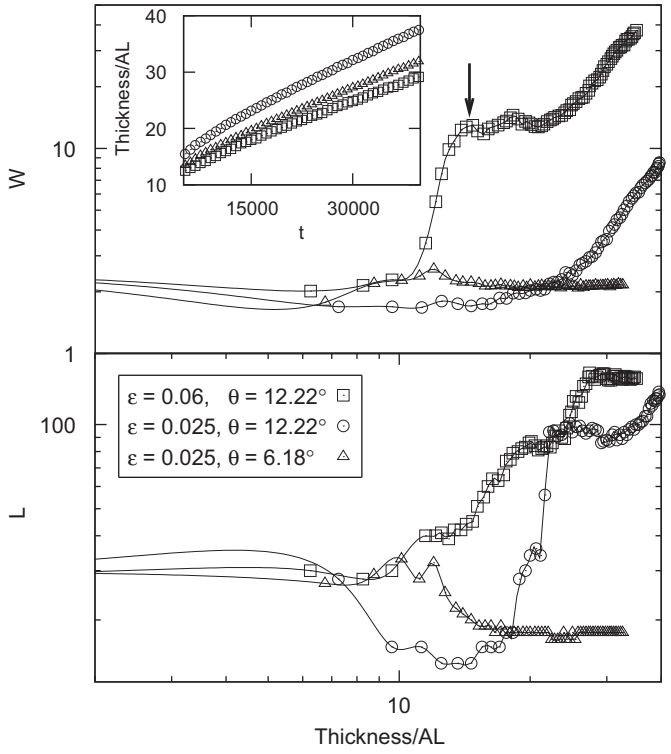

Fig. 5. The surface roughness W and the correlation length L versus the film thickness with square, circle, and triangular corresponding to Fig. 4(a), (b), and (c), respectively. Inset: the film thickness increases with the time t.

hill-and-valley structure (square) and the step-bunching structure (circle). In contrast, W and L both reach constant states, indicating a stable growth of the regular step-flow structure (triangular). For larger ε, the oscillation of W can tell the critical film thickness H_c of the mismatch dislocation nucleation (see the arrow in Fig. 5). We compare the film growth velocity in the inset of Fig. 5. The step-bunching structure is of larger growth velocity, while the hill-and-valley facet structure and the regular step-flow structure are of slower growth velocities. Consider the former corresponds to the larger step density as compared with the latter, we can suppose that the solid prefers growing at the stepped surface. The singular surfaces are also found to grow slowly due to the low step density, which explains why the stable morphologies are obtained for small ε.

As shown in Figs. 4 and 5, the growth kinetics is involved in the advancing film growth front, which changes the value of the mismatch strain at the border of different morphological regimes, as compared with the morphological phase-diagram shown in Fig. 3. For example, the film growth advancing with a constant velocity indicates a larger critical values of the mismatch strain at the border between the regular step train and the step bunching as well as between the step bunching and the hill-and-valley structure, but indicates less critical values that the mismatch dislocations are caused. We find that more mismatch dislocations are caused during the growing strained film, which corresponds to a less critical value of ε that the mismatch dislocation is caused. For example, the mismatch dislocation is absent until $\varepsilon>0.06$ during the near-equilibrium film growth on the vicinal substrate of $\theta=12.22^{\circ}$, whereas the mismatch dislocation is caused when $\varepsilon>0.02$ in the corresponding case during the film growth with the constant velocity. This critical value of ε for the mismatch dislocation formation is reflected by the starting point of the linear relationship of $P\sim\varepsilon$, wherein $P=[1+\log_{10}(H_c)]/H_c$, that is

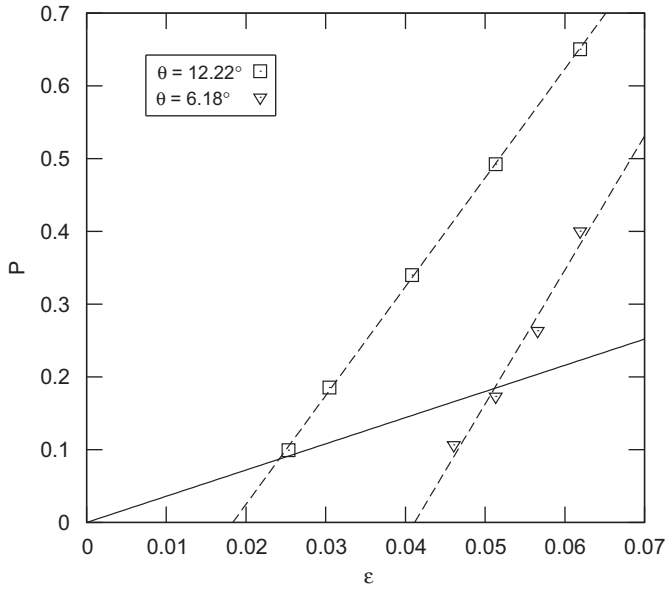

Fig. 6. Mismatch dislocation nucleation of the heteroepitaxial growth, wherein $P=[1+\log(H_c)]/H_c$ and H_c is the critical film thickness that the mismatch dislocation nucleates, which changes with the mismatch strain ε and the vicinal angle θ. The solid line refers to the heteroepitaxial growth on the singular substrate simulated based on diffusive PFC surfaces [18].

plotted in Fig. 6. The critical ε values around $\varepsilon=0.02$ and 0.04 are indicated, corresponding to the cases of $\theta=12.22^{\circ}$ (square) and $\theta=6.18^{\circ}$ (triangular), respectively. In Fig. 6, we compare the results of $P\sim\varepsilon$ obtained for the heteroepitaxial growth on the vicinal substrate (square and triangular) and the reported result

(solid line) for heteroepitaxial growth on a singular substrate but with the diffusive PFC surface [18]. While the coherent film growth is obtained below the critical ε values, P is far larger than the referred data based on the diffusive PFC surface in the regime of large ε. This difference is attributed to the steps and their unstable growth occurring on the sharp PFC surface, which is absent on the diffusive PFC surface. In the cases of small ε, the stepped structure is dominant on the surface, the mismatch strain energy can be released through a local distortion of atomic lattices of steps or through a surface undulation in the step-bunching mode, which contributes to the coherent growth of the heteroepitaxial growth on the vicinal substrate. However, in the cases of large ε values, the hill-and-valley structure is caused by the step faceting, on which atomic closed-packed face the only way to release the mismatch stain energy is dislocation nucleation. This increases the possibility of the mismatch dislocation formation, which explains a high P for the heteroepitaxial growth on the vicinal substrate in the regime of large ε values.

4. Conclusions

The morphological instabilities of the heteroepitaxial growth on the vicinal substrate are investigated using PFC simulations based on sharp solid–liquid interface. The 3D PFC simulation captures the atomistic details, the large-scale morphology as well as the mismatch dislocations within the film successfully. Diverse morphologies such as equally spaced step trains, bunched step trains and hill-and-valley facetted structure with or without dislocations are reproduced as functions of the mismatch strain and the vicinal angle. The film growth with an constant velocity indicates a less critical film thickness H_c that the mismatch dislocations arise up, as compared with the film growth near equilibrium. The coherent film growth is dominated due to the step-flow and the step-bunching growth modes in the regime of small ε. However, the non-coherent film growth tendency becomes greatly strong in the regime of large ε, caused by the increased possibility of the mismatch dislocation formation that is companied by the island nucleation and the growth on the hill-and-valley facetted surface. The simulation results indicate that the steps, the islands, and the mismatch dislocation are interconnected during the heteroepitaxial growth on the vicinal substrate.

Acknowledgements

This work has been partially supported by EU FP6, through NMP STRP 016447 "MagDot", by DFG through SFB 609 and Yound Research Academy on Materials Science (Grant no. Ra 1850/1-1), by Nature Science Foundation of China (Grant no. 10974228).

Appendix A. Supplementary material

Supplementary data associated with this article can be found in the online version of 10.1016/j.jcrysgro.2010.08.047.

References

[1] R.J. Asaro, W.A. Tiller, Metall. Trans. 3 (1972) 1789.
[2] M.A. Grinfeld, J. Nonlinear Sci. 3 (1993) 35.
[3] B.J. Spencer, P.W. Voorhees, S.H. Davis, Phys. Rev. Lett. 67 (1991) 3696.
[4] M. Haataja, J. Müller, A.D. Rutenberg, M. Grant, Phys. Rev. B 65 (2001) 035401.
[5] S.M. Wise, J.S. Lowengrub, J.S. Kim, K. Thornton, P.W. Voorhees, Appl. Phys. Lett. 87 (2005) 133102.
[6] A. Rätz, A. Ribalta, A. Voigt, J. Comput. Phys. 214 (2006) 187.
[7] C. Duport, P. Politi, J. Villain, J. Phys. I 5 (1995) 1317.
[8] F. Haußer, M.E. Jabbour, A. Voigt, Multiscale Model. Simul. 6 (2007) 158.
[9] X.B. Niu, Y.-J. Lee, R.E. Caflisch, C. Ratsch, Phys. Rev. Lett. 101 (2008) 086103.
[10] M.T. Lung, C.H. Lam, L.M. Sander, Phys. Rev. Lett. 95 (2005) 086102.
[11] R. Zhu, E. Pan, P.W. Chung, Phys. Rev. B 75 (2007) 205339.
[12] J.N. Aqua, T. Frisch, Phys. Rev. B 78 (2008) 121305(R).
[13] T.P. Schulze, P. Smereka, J. Mech. Phys. Solids 57 (2009) 521.
[14] F. Much, M. Biehl, Europhys. Lett. 63 (2003) 14.
[15] S.P.A. Gill, T. Wang, Surf. Sci. 602 (2008) 3560.
[16] F. El-Mellouhi, N. Mousseau, L.J. Lewis, Phys. Rev. B 78 (2008) 153202.
[17] K.R. Elder, M. Katakowski, M. Haataja, M. Grant, Phys. Rev. Lett. 88 (2002) 245701.
[18] K.R. Elder, M. Grant, Phys. Rev. E 70 (2004) 051605.
[19] A. Jaatinen, C.V. Achim, K.R. Elder, T. Ala-Nissila, Phys. Rev. E 80 (2009) 031602.
[20] G. Tegze, L. Granasy, G.I. Toth, F. Podmaniczky, A. Jaatinen, T. Ala-Nissila, T. Pusztai, Phys. Rev. Lett. 103 (2009) 035702.
[21] C.V. Achim, M. Karttunen, K.R. Elder, E. Granato, T. Ala-Nissila, S.C. Ying, Phys. Rev. E 74 (2006) 021104.
[22] R. Backofen, A. Rätz, A. Voigt, Philos. Mag. Lett. 87 (2007) 813.
[23] K.R. Elder, N. Provatas, J. Berry, P. Stefanovic, M. Grant, Phys. Rev. B 75 (2007) 064107.
[24] R. Backofen, A. Voigt, J. Phys. Condens. Matter 21 (2009) 464109.
[25] A. Pimpinelli, J. Villain, Physics of Crystal Growth, Cambridge University Press, 1998.
[26] G.M. Watson, D. Gibbs, D.M. Zehner, M. Yoon, S.G.J. Mochrie, Phys. Rev. Lett. 71 (1993) 3166.